Compact Solid-State 213 nm Laser Enables Standoff Deep Ultraviolet Raman Spectrometer: Measurements of Nitrate Photochemistry

Sergei V. Bykov,[a] Michael Mao,[b] Katie L. Gares,[a] Sanford A. Asher[a,*]

[a] *University of Pittsburgh, Department of Chemistry, Pittsburgh, PA 15260 USA*
[b] *UVisIR Inc., Suite 102, 23600 Mercantile Road, Beachwood, OH 44122 USA*

We describe a new compact acousto-optically Q-switched diode-pumped solid-state (DPSS) intracavity frequency-tripled neodymium-doped yttrium vanadate laser capable of producing ~100 mW of 213 nm power quasi-continuous wave as 15 ns pulses at a 30 kHz repetition rate. We use this new laser in a prototype of a deep ultraviolet (UV) Raman standoff spectrometer. We use a novel high-throughput, high-resolution Echelle Raman spectrograph. We measure the deep UV resonance Raman (UVRR) spectra of solid and solution sodium nitrate ($NaNO_3$) and ammonium nitrate (NH_4NO_3) at a standoff distance of ~2.2 m. For this 2.2 m standoff distance and a 1 min spectral accumulation time, where we only monitor the symmetric stretching band, we find a solid state $NaNO_3$ detection limit of ~100 μg/cm^2. We easily detect ~20 μM nitrate water solutions in 1 cm path length cells. As expected, the aqueous solutions UVRR spectra of $NaNO_3$ and NH_4NO_3 are similar, showing selective resonance enhancement of the nitrate (NO_3^-) vibrations. The aqueous solution photochemistry is also similar, showing facile conversion of NO_3^- to nitrite (NO_2^-). In contrast, the observed UVRR spectra of $NaNO_3$ and NH_4NO_3 powders significantly differ, because their solid-state photochemistries differ. Whereas solid $NaNO_3$ photoconverts with a very low quantum yield to $NaNO_2$, the NH_4NO_3 degrades with an apparent quantum yield of ~0.2 to gaseous species.

Index Headings: **Compact laser; Standoff spectrometer; Ultraviolet; UV; Deep UV Raman; UV resonance Raman; UVRR; Nitrate photochemistry; Standoff detection; Explosives detection.**

INTRODUCTION

An important advantage of Raman spectroscopy is its ability to remotely identify chemical substances based on their unique vibrational signatures.[1–9] The detection ability of Raman spectroscopy is mainly limited by the inherent weakness of the Raman effect since only a small fraction of the scattered light exchanges energy with the vibrational states of the irradiated molecules. This inelastically scattered light carries information about molecular structure. In addition, only a small fraction of scattered light can be monitored and analyzed if the Raman spectra are measured remotely. This decreases the sensitivity of standoff Raman measurements, making detection of trace quantities difficult.

Excitation of the Raman spectra in the deep ultraviolet (UV) can give rise to a significantly increased selectivity and sensitivity of Raman measurements due to the resonance enhancement, the ν^4 dependence of Raman scattering intensity, and the lack of fluorescent interference in this spectral region.[10] Ultraviolet resonance Raman excitation has been shown to be advantageous for detecting trace explosive materials.[3,11–13]

The development of deep UV standoff spectrometers has been slowed by the lack of suitable deep UV lasers.[14] Optimal excitation wavelengths are crucial for UV resonance Raman (UVRR) measurements since Raman band cross sections, sampling volumes, and photochemistry significantly depend on excitation wavelength. Today, UV Raman excitation usually uses neodymium-doped yttrium aluminum garnet third (355 nm), fourth (266 nm), and fifth (213 nm) harmonics, or the second harmonics of visible Ar-ion laser lines at 257, 248, 244, and 229 nm or UV-tunable (193–240 nm) fourth harmonics of the Ti:Sapphire oscillators. These lasers show 2–20 mW output powers below 244 nm. These lasers can only be used as a part of stationary Raman spectrometers since they are large and heavy, require water cooling, and have electrically inefficient power supplies. High-power low-duty cycle excimer lasers, such as ArF at 193 nm and KrF at 248 nm require, use of reactive halogen-containing gases. Standoff Raman instruments would best use small, portable, high-electrical power-efficient UV lasers.

In this study, we report on the development of a new compact solid-state deep UV (213 nm) laser that will find application in compact standoff deep UV Raman instruments. We demonstrate deep UV Raman spectral standoff measurements of solid and solution sodium nitrate ($NaNO_3$) and ammonium nitrate (NH_4NO_3) at distances of ~2.2 m. We also examine the photochemistry of nitrates that occur with 213 nm excitation.

Received 26 March 2015; accepted 17 April 2015.
* Author to whom correspondence should be sent. E-mail: asher@pitt.edu.
DOI: 10.1366/15-07960

0003-7028/15/6908-0895/0
© 2015 Society for Applied Spectroscopy

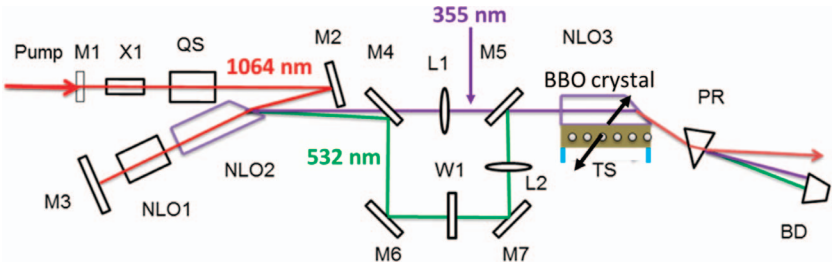

FIG. 1. Optical layout of the 213 nm DPSS Nd : YVO_4 laser. M1, pump mirror; M2, cavity fold mirror; M3, cavity end mirror; M4–M7, 532/355 separator; L1; focal lens for 355 nm laser; L2, focal lens for 532 nm laser; NLO1, second harmonic crystal; NLO2, third harmonic crystal; NLO3, fifth harmonic crystal; X1, $NdYVO_4$ laser crystal; QS, Q-switch; PR, beam separator prism; BD, beam dumper; W1, half-wave plate for 532 nm light; TS, translation stage. The BBO crystal is constantly moving back and forth at the speed of 50 μm/s.

Our 213 nm laser excitation falls within absorption bands of many energetic molecules since nitro (-NO_2) and nitrate ester (ONO_2) groups as well as nitrate anions (NO_3-) found in explosives absorb strongly around 213 nm. This 213 nm UV excitation gives rise to significant resonance enhancement of molecules, such as nitrates, trinitrotoluene (TNT), pentaerythritol tetranitrate (PETN), and cyclotrimethylene trinitramine (RDX).[11]

INSTRUMENTATION

The 213 nm UV Laser. The 213 nm laser shown in Fig. 1 was designed and manufactured by UVisIR Inc. (Beachwood, OH). It consists of an acousto-optically Q-switched, diode-pumped solid-state (DPSS) neodymium-doped yttrium vanadate (Nd:YVO_4) laser that is frequency quintupled to 213 nm. It operates at a 30 kHz repetition rate, generating 15 ns pulses at the 1064 nm fundamental. Although Nd:YVO_4 has been long known as a laser medium,[15] it became popular only recently due to advances in the ability to manufacture high-quality optical crystals. Nd:YVO_4 has one of the highest stimulated emission cross sections among laser crystals,[16] and it is capable of operation at high repetition rates, from kilohertz to megahertz. Its broad and strong 808.5 nm absorption band often eliminates the necessity for pump wavelength stabilization. All of these reasons make Nd : YVO_4 an ideal material for compact, high-efficient, and high-power DPSS lasers.

Figure 1 shows the optical diagram of the 213 nm DPSS laser. The pump diodes lase at 808 nm to match the maximum absorbance of the Nd^{3+} in the Nd : YVO_4 crystal (X1). Lasing generates the 1064 nm fundamental. The X1 is cooled by water at 18 °C. The horizontally polarized 1064 nm light is intracavity tripled in the folded cavity formed by mirrors M1, M2, and M3. The second harmonic crystal (NLO1) is a type I phase-matched crystal that doubles the fundamental frequency. This generates vertically polarized 532 nm light. The third harmonic crystal (NLO2) is a type I phase-matched crystal that mixes the fundamental and second harmonic frequencies to generate horizontally polarized 355 nm light. Both NLO1 and NLO2 are lithium triborate crystals that are maintained at a constant temperature thermoelectrically. Wedged NLO2 acts as a prism to separate the 1064, 532, and 355 nm laser beams. Crystals X1, NLO1, and NLO2 are anti-reflection coated for 1064 and 532 nm light. The conversion efficiency for NLO1 is ~40% and for NLO2 is ~20%.

The 355 nm third harmonic is mixed with the 532 nm second harmonic to generate 213 nm light. The dichroic mirror M4 reflects the 532 nm light and mirror M6 passes it through the half-wave plate to rotate the 532 nm light polarization 90°. M7 passes 532 nm light through lens L2 that focuses it inside the fifth harmonic barium borate (BBO) crystal. The mirror reflection efficiency is >99.5% and lens losses are <1%.

The final sum-frequency generating stage mixes both horizontally polarized third harmonic 355 nm and the second harmonic 532 nm light through the fifth harmonic generation BBO crystal (NLO3) to produce vertically polarized 213 nm light with ~10% efficiency. The BBO crystal is on a translation stage that is continuously moving across the laser beam at 50 μm/s to avoid BBO crystal degradation. Typical output powers are shown in Table I. The laser generates ~100 mW of 213 nm light at a 26 A diode current.

Laser Size and Weight. The laser head is compact in size and weighs < 10 kg. Its dimensions are ~ 48 × 16 × 11 cm (length × width × height).

The laser power supply is ~ 43 × 20 × 9 cm. The laser is cooled by using a closed loop cooling system. The cooling system is ~ 19 × 13 × 17 cm. The cooling water temperature is 18 °C and the flow rate is ~0.5 L/min.

Standoff Ultraviolet Raman Spectrometer. For standoff measurements, we used our lab-built high-throughput, high-resolution Echelle deep-UV Raman spectrometer.[17] Samples were measured at 2.2 m standoff distance using a backscattering sampling geometry. The laser beam was focused to an ~2 mm spot on the rotating sample of ~1 cm^2 area. The scattered light was collected by a 5 cm diameter plano-convex fused silica lens and focused onto the spectrograph entrance slit. Accumulation times varied from

TABLE I. Output powers for DPSS Nd : YVO_4 213 nm laser.

Current (A)	213 laser power (mW)
23	~30
24	~65
25	~80
26	~100

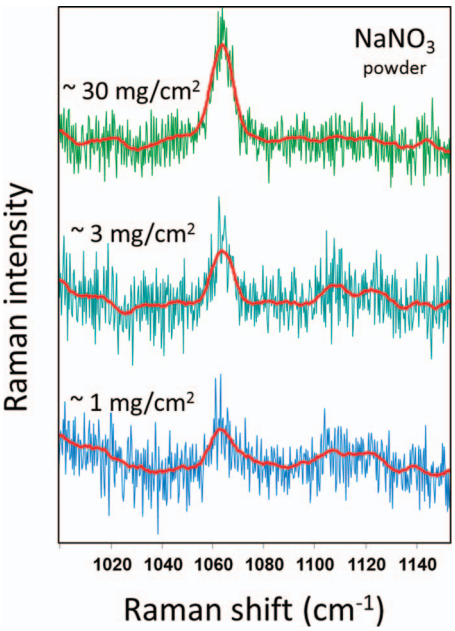

FIG. 2. Standoff 213 nm UVRR spectra of different quantities of solid $NaNO_3$ powder on the bottom of rotating cell groove (~1 cm^2 total area). The 2.2 m standoff distance, 60 s accumulation time, incident irradiance is ~30 mW/cm^2. Raw and smoothed (Savitzky–Golay) spectra are overlaid.

~10 s to ~5 min. The incident 213 nm light irradiance on a rotating sample for standoff measurements was ~30 mW/cm^2.

To compare the $NaNO_3$ and NH_4NO_3 213 nm photochemistry, we measured non-standoff UV Raman spectra of solid and solution nitrate samples after extensive irradiation with 213 nm light. These non-standoff measurements used spectrographs described previously.[18,19] Spectra were detected using a liquid nitrogen cooled charge-coupled device camera (Spec-10, Princeton Instruments). For non-standoff measurements, we used a 213 nm incident irradiance on a rotating sample of ~130 mW/cm^2.

Samples. The solid-state UVRR measurements of NH_4NO_3 and $NaNO_3$ (J.T. Baker) used samples crushed into fine powders that were compacted into the groove of a rotating cell. For the detection limit measurements, a small amount (~1 and ~3 mg) of the fine $NaNO_3$ powder inside the groove of the metal rotating cell (~1 cm^2 surface area) was moistened with 200 proof ethanol (Decon Laboratories). After drying, the nitrate powder adhered to the groove bottom surface.

For the mass change measurements, we used dense melted nitrate samples. Approximately 50 mg of NH_4NO_3 and $NaNO_3$ powders were heated ~10 °C above their melting points inside small Teflon cups and then slowly cooled to room temperature.

For solution measurements, nitrates were dissolved in water at 2 M, 0.5 M, 0.02 M, 2 mM, 0.2 mM, and 0.02 mM concentrations. Raman spectra of solution samples were measured in a 1 cm path length fused silica capped cuvette that was continuously stirred with a magnetic stir bar.

SOLID NITRATES

The strong ~200 nm nitrate (NO_3^-) $\pi \rightarrow \pi^*$ electronic transition strongly enhances the NO_3^- stretching vibrations.[11] Figure 2 shows the 213 nm excited standoff UV Raman spectra of the NO_3^- symmetric stretching vibration ($\nu 1$) obtained from samples where different amounts of $NaNO_3$ powder adhered to the bottom of the rotating cell groove. In this experiment, the laser beam was focused to an ~2 mm diameter spot to exactly illuminate the width of the rotating groove, which had a total area of ~1 cm^2.

The $\nu 1 NO_3^-$ vibration gives rise to an intense UV resonance Raman band at ~1065 cm^{-1}. At a 2.2 m standoff distance, this band is clearly detectable in the UVRR spectrum of 1 mg/cm^2 nitrate powder with 60 s spectral accumulation time (see Fig. 2). We estimate a detection limit for these 1 min measurements monitoring only the $\nu 1 NO_3^-$ vibration of ~100 $\mu g/cm^2$.

We irradiated nitrate powders for extended times to investigate the effect of photochemistry on the UVRR spectra. Figure 3 shows the 213 nm excited standoff UVRR of the NO_3^- symmetric stretching vibrations of $NaNO_3$ and NH_4NO_3 powders. The $\nu 1$ of solid NH_4NO_3 is at ~1045 cm^{-1}, whereas that of solid $NaNO_3$ is at ~1065 cm^{-1}. We previously demonstrated that illumination of solid $NaNO_3$ within its 200 nm absorption band results in formation of nitrite (NO_2^-) and molecular oxygen.[20] This solid-state photodecomposition perturbs the NO_3^- at crystal lattice sites adjacent to the photolyzed NO_3^-. This results in ~13 cm^{-1} upshift of the $\nu 1$ symmetric Raman band frequency. For a 213 nm UV irradiance of ~30 mW/cm^2, the upshifted $\nu 1(NO_3^-)$ band at ~1078 cm^{-1} appears in UVRR spectra after ~15 min irradiation (Fig. 3). After ~25 min, the ~1078 cm^{-1} band intensity becomes larger than that the unperturbed ~1068 cm^{-1} band.

In contrast to $NaNO_3$, the NH_4NO_3 UV Raman spectrum does not similarly change with extended UV irradiation (Fig. 3). This indicates that significantly different solid-state photochemistry occurs for NH_4NO_3 compared to $NaNO_3$.

To gain insight into UV photochemistry of $NaNO_3$ and NH_4NO_3, we irradiated these powders with ~130 mW/cm^2 of 213 nm laser light over different time periods (Fig. 4). As the UV irradiation exposure of $NaNO_3$ increases, the NO_3^- Raman band intensities decrease. This includes the $\nu 1$ at ~1068 cm^{-1}, $\nu 3$ at ~1385 cm^{-1}, overtone of $\nu 2$ at ~1670 cm^{-1}, and overtone of $\nu 1$ at ~2133 cm^{-1}, indicating $NaNO_3$ decomposition. At the same time, the photoproduct NO_2^- Raman bands at ~1331 and ~2654 cm^{-1} increase.[20]

In contrast, the NH_4NO_3 UVRR spectrum (Fig. 4) does not change upon UV irradiation as we observed with the Fig. 3 standoff measurements. Given that we show below that the sample weight decreases upon 213 nm excitation, we presume that the UV-induced decomposition products are gaseous and do not redeposit on the NH_4NO_3 surface.

Ultraviolet-induced decomposition of ammonium nitrate can be a complex process and may follow one or more of the pathways of its thermal decomposition, which give rise to ammonia (NH_3), nitrous oxide (N_2O),

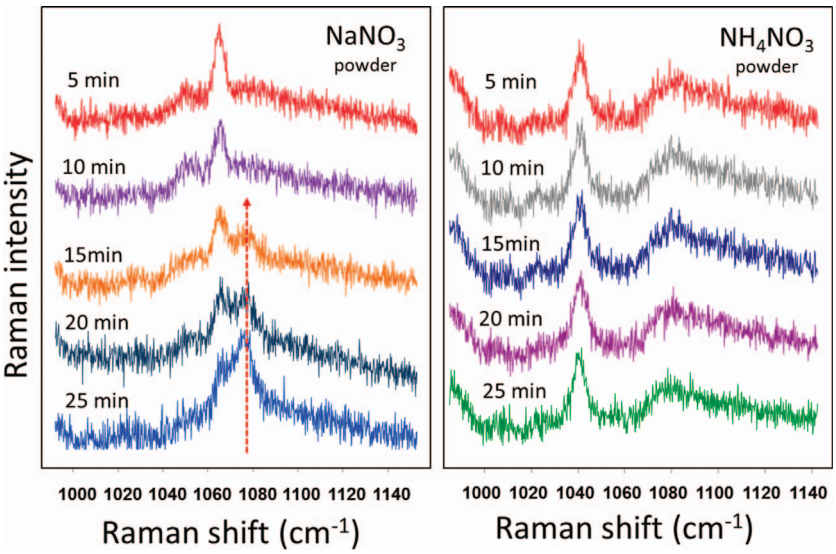

FIG. 3. Standoff 213 nm UV resonance Raman spectra of solid $NaNO_3$ and NH_4NO_3 (~100 mg/cm^2) at different irradiation times. Incident irradiance on a rotating sample is ~30 mW/cm^2. The 2.2 m standoff distance, 5 min spectral accumulation times.

nitrogen dioxide (NO_2), nitric oxide (NO), nitrogen gas(N_2), oxygen gas (O_2), and water (H_2O):[21]

$$NH_4NO_3 \rightarrow NH_3 + HNO_3 \quad (1)$$

$$NH_4NO_3 \rightarrow N_2O + 2H_2O \quad (2)$$

$$NH_4NO_3 \rightarrow 3/4N_2O + 1/2NO_2 + 2H_2O \quad (3)$$

$$NH_4NO_3 \rightarrow N_2 + 2H_2O + 1/2O_2 \quad (4)$$

$$8NH_4NO_3 \rightarrow 5N_2 + 4NO + 2NO_2 + 16H_2O \quad (5)$$

$$NH_4NO_3 \rightarrow 1/2N_2 + NO + 2H_2O \quad (6)$$

We directly monitored conversion of NH_4NO_3 to gaseous species and determined the apparent quantum yield by measuring the mass loss of $NaNO_3$ and NH_4NO_3 samples irradiated with 213 nm light. Figure 5 shows the dependence of the mass of solid $NaNO_3$ and NH_4NO_3 samples resulting from irradiation with ~50 mW of 213 nm laser light focused to ~1 mm spot for 2 h.

For this experiment, ~50 mg of solid nitrate was melted in a small Teflon cup to create a dense polycrystalline solid. The sample irradiated was situated on a balance where it was continuously weighed. We estimate a steady-state sample temperature increase under laser irradiation of ~5 °C.[22] To rule out the possibility of NH_4NO_3 mass decrease due to sublimation, we heated the NH_4NO_3 sample at 100 °C for ~2 h without UV irradiation, periodically weighing it. We observed no mass change within measurement error ±0.1 mg.

Dramatically different weight loss behaviors were seen in the $NaNO_3$ and NH_4NO_3. The $NaNO_3$ mass drops by only ~1 mg over the first 60 min, after which the

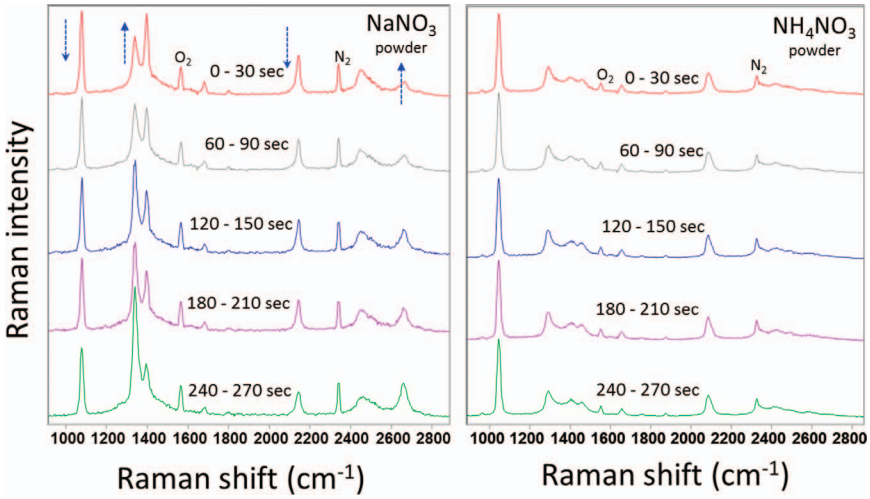

FIG. 4. The 213 nm UVRR spectra of $NaNO_3$ and NH_4NO_3 powders at different irradiation times. Incident irradiance on a rotating sample is ~130 mW/cm^2, 30 s accumulation times. Spectra are scaled to stretching band of molecular N_2 (air).

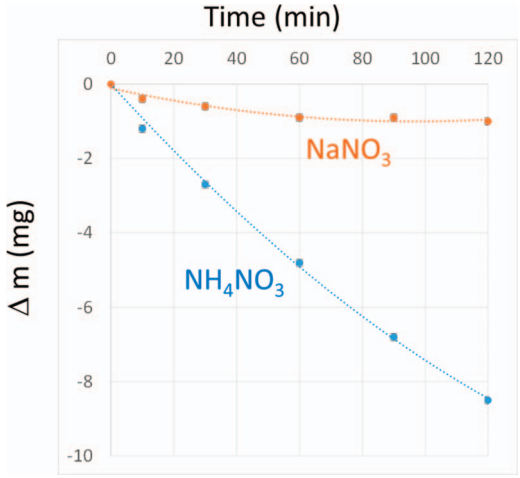

FIG. 5. Mass change of the solid $NaNO_3$ and NH_4NO_3 samples upon UV irradiation. The incident irradiance at 213 nm is ~5 W/cm^2 (~50 mW focused to ~1 mm^2). The weighing error is ±0.1 mg. Error bars are smaller than symbols.

weight stabilizes. This small mass loss probably is due to ablation of material from loss of O_2 from the $NaNO_3$ close to the surface of the sample due to the buildup of pressure, as we observed previously.[20] Our previous measurements of the photochemical quantum yield of solid $NaNO_3$ indicates a very small quantum yield (10^{-8}) for formation of NO_2^- and O_2.

In contrast, the mass of NH_4NO_3 sample decreases almost linearly, with apparent rate of ~30 ng·s^{-1}·mW^{-1}. For the rate calculation, we assume linear dependence of NH_4NO_3 mass from irradiation time for the first three time points. This corresponds to an apparent quantum yield for conversion of solid NH_4NO_3 into gaseous product of ~0.20 ± 0.02. This is a much higher quantum yield than for $NaNO_3$. As shown below, it is comparable to the nitrate photolysis quantum yields in aqueous solutions.

PHOTOCHEMISTRY OF AQUEOUS NITRATE SOLUTIONS

Aqueous solutions of $NaNO_3$ and NH_4NO_3 show identical UVRR spectra that are dominated by NO_3^- vibrations, their overtones, and combination bands. The NO_3^- are fully hydrated and isolated from their counter ions. As in the solid state, the strongest band at ~1044 cm^{-1} results from the $\nu 1 NO_3^-$ symmetric stretching vibration. It is clearly detectable at ~10 s accumulation times even for 20 μM solution concentrations.

The observed solution 1044 cm^{-1} Raman band intensities are essentially independent of NH_4NO_3 concentration over the 2 M– 0.2 mM (in the 16 parts per million [ppm]) range (Figs. 6A and 6B). This is because we have a large depth of focus for our collection optics and because the total resonance Raman intensities are determined by the intensity of the excitation beam within the sample. Figures 6C and 6D show the 213 nm laser beam attenuation due to sample absorption calculated from our measured 213 nm extinction coefficient of NH_4NO_3 in water. At high concentrations, the excitation beam is completely absorbed within a thin surface layer of solution; in 2 M NH_4NO_3 solution the 213 nm beam penetrates only ~1 μm. As the concentration decreases, the laser beam penetrates deeper, which increases the sampled volume. Thus, the number of irradiated molecules remains constant, and the UV resonance Raman intensity of the 1044 cm^{-1} Raman band is constant. For a 1 cm path length cell, the 213 nm laser beam is completely absorbed down to 0.2 mM concentration (Fig. 6). At 20 μM (1.6 ppm), NH_4NO_3 concentration ~70% of 213 nm excitation passes through the 1 cm cell, resulting in a significantly decreased 1044 cm^{-1} band Raman intensity.

We compared the 213 nm aqueous solution photochemistry of $NaNO_3$ and NH_4NO_3. Figure 7A provides UV resonance Raman spectra of $NaNO_3$ and NH_4NO_3 in water, showing the initial spectra as well as samples irradiated with ~40 mW of 213 nm laser light for 30 and 60 min. The solutions of $NaNO_3$ and NH_4NO_3 show essentially identical spectral changes upon UV photolysis. Bands due to NO_3^- vibrations ($\nu 1$ at ~1047 cm^{-1}, $\nu 3$ at ~1336 cm^{-1}, overtone of $\nu 2$ at ~1664 cm^{-1}, overtone of $\nu 1$ at ~2096 cm^{-1}) decrease in intensity over time. At the same time, two new peaks at 1331 and 2654 cm^{-1} appear and become more intense over time, indicating formation of NO_2^-, as it is clearly confirmed by difference spectra between the irradiated samples and initial spectrum (Figs. 7B and 7C). Although the photochemistry of NH_4NO_3 and $NaNO_3$ differ in the solid state, they are identical in aqueous solution, presumably because the NH_4^+ counter ion is distant from the excited hydrated NO_3^-.

CONCLUSIONS

We developed a new compact DPSS 213 nm laser as an excitation source for deep UV standoff Raman instruments and used it in a high-efficiency standoff Raman spectrometer. We used it to monitor the deep UV resonance Raman spectra of solid and solution nitrate species. At ~2.2 m standoff distance, we were able to monitor easily the NO_3^- symmetric stretching band in the UVRR spectrum of 1 mg/cm^2 nitrate powder spread on a metal surface or down to 20 μM solution in water. For the solid NH_4NO_3, we estimate a detection limit for a 1 min spectral accumulation of ~100 μg/cm^2. We find similar solution state $NaNO_3$ and NH_4NO_3 213 nm photochemistry. The hydrated NO_3^- photodecomposes to NO_2^-.

In contrast, solid state $NaNO_3$ and NH_4NO_3 show different UV photochemistry. Solid $NaNO_3$ decomposes into $NaNO_2$ and O_2, which degrades the $NaNO_3$ crystal structure and upshifts the $\nu 1$ vibration of NO_3^- from ~1065 to ~1078 cm^{-1}. The nitrite band becomes more intense as the photolysis extent increases. In contrast to $NaNO_3$, solid NH_4NO_3 shows no change in its UVRR spectrum, even after prolonged exposure to UV light because the NH_4NO_3 decomposes into gaseous products.

We also measured the rate of solid NH_4NO_3 UV-induced mass loss (~30 ng·s^{-1}·mW^{-1}) to determine an apparent quantum yield of ~0.20 ± 0.02, which is close to that of nitrate in water. This is much lower than our previously measured quantum yield of ~10^{-8} of solid-state $NaNO_3$.

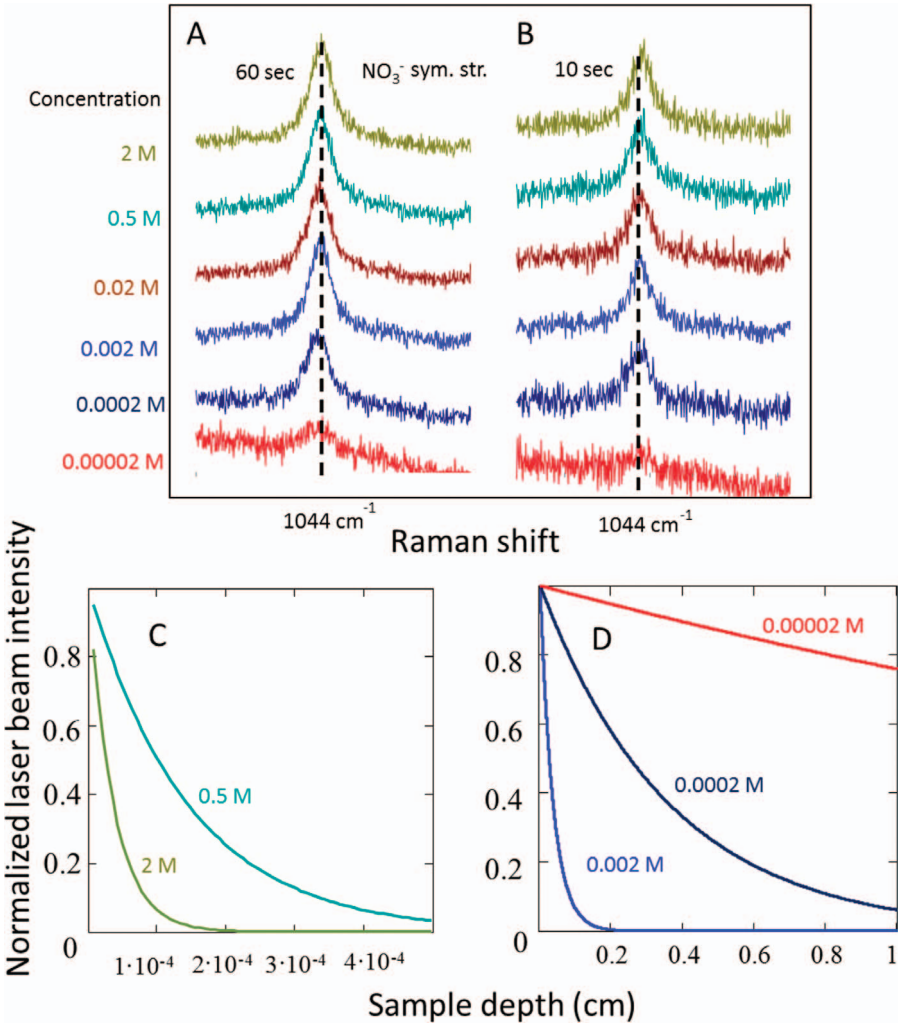

FIG. 6. The 213 nm UVRR spectra of NH_4NO_3 aqueous solutions at different concentrations measured at ~2.2 m standoff distance in a 1 cm path length cell: (**A**) 60 s accumulation time and (**B**) 10 s accumulation time. (**C**) and (**D**) Calculated depth profiles of laser beam intensity due to sample absorption for different NH_4NO_3 concentrations.

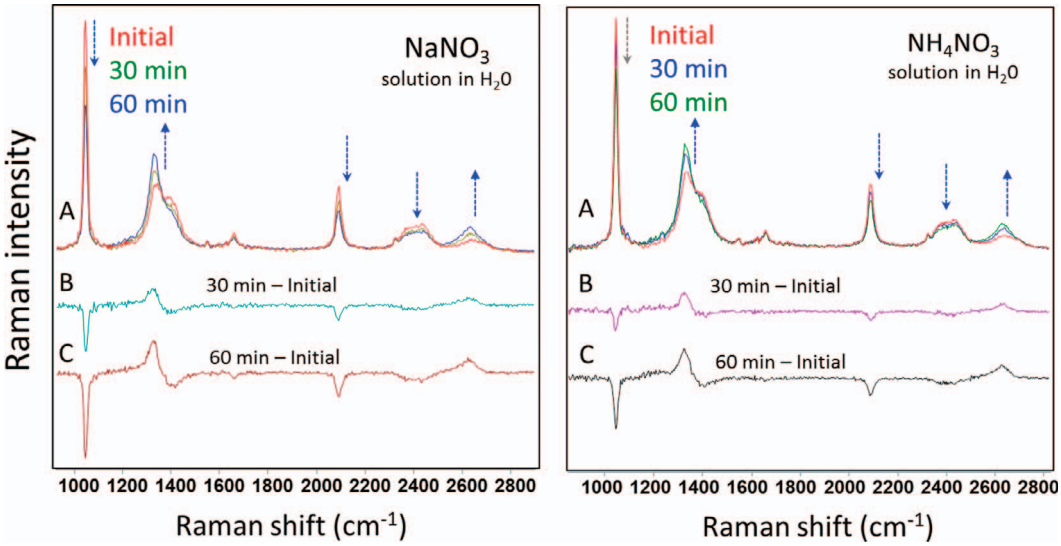

FIG. 7. (***A***) UVRR spectra (non-standoff) of water solution of $NaNO_3$ and NH_4NO_3 at different irradiation times: initial, 30 and 60 min. (***B***) Difference spectrum between irradiated for 30 min and initial spectrum. (***C***) Difference spectrum between irradiated for 60 min and initial spectrum. Difference spectra show photolysis of NO_3^- (negative features) and formation of NO_2^- (positive features) for both $NaNO_3$ and NH_4NO_3 in solution.

ACKNOWLEDGMENT

This work was supported by an Office of Naval Research (ONR) N00014-12-1-0021 contract.

1. J.C. Carter, S.M. Angel, M. Lawrence-Snyder, J. Scaffidi, R.E. Whipple, J.G. Reynolds. ''Standoff Detection of High Explosive Materials at 50 Meters in Ambient Light Conditions Using a Small Raman Instrument''. Appl. Spectrosc. 2005. 59(6): 769-775.
2. L.C. Pacheco-Londoño, W. Ortiz-Rivera, O.M. Primera-Pedrozo, S.P. Hernández-Rivera. ''Vibrational Spectroscopy Standoff Detection of Explosives''. Anal. Bioanal. Chem. 2009. 395(2): 323-335.
3. D.D. Tuschel, A.V. Mikhonin, B.E. Lemoff, S.A. Asher. ''Deep Ultraviolet Resonance Raman Excitation Enables Explosives Detection''. Appl. Spectrosc. 2010. 64(4): 425-432.
4. S.M. Angel, N.R. Gomer, S.K. Sharma, C. McKay. ''Remote Raman Spectroscopy for Planetary Exploration: A Review''. Appl. Spectrosc. 2012. 66(2): 137-150.
5. A.K. Misra, S.K. Sharma, T.E. Acosta, J.N. Porter, D.E. Bates. ''Single-Pulse Standoff Raman Detection of Chemicals from 120 M Distance During Daytime''. Appl. Spectrosc. 2012. 66(11): 1279-1285.
6. E.L. Izake, B. Cletus, W. Olds, S. Sundarajoo, P.M. Fredericks, E. Jaatinen. ''Deep Raman Spectroscopy for the Non-Invasive Standoff Detection of Concealed Chemical Threat Agents''. Talanta. 2012. 94: 342-347.
7. A. Ehlerding, I. Johansson, S. Wallin, H. Östmark. ''Resonance-Enhanced Raman Spectroscopy on Explosives Vapor at Standoff Distances''. Int. J. Spectrosc. 2012. 158715.
8. S.K. Sharma, J.N. Porter, A.K. Misra, C.E. Helsley, D.E. Bates. ''Scanning Time-Resolved Standoff Raman Instrument for Large-Area Mineral Detection on Planetary Surfaces''. Eur. J. Mineral. 2013. 25(5): 715-720.
9. M. Skulinova, C. Lefebvre, P. Sobron, E. Eshelman, M. Daly, J.F. Gravel, J.F. Cormier, F. Châteauneuf, G. Slater, W. Zheng, A. Koujelev, R. Léveillé. ''Time-Resolved Stand-Off UV-Raman Spectroscopy for Planetary Exploration''. Planet. Space Sci. 2014. 92: 88-100.
10. S.A. Asher, C.R. Johnson. ''Raman Spectroscopy of a Coal Liquid Shows that Fluorescence Interference is Minimized with Ultraviolet Excitation''. Science. 1984. 225(4659): 311-313.
11. M. Ghosh, L. Wang, S.A. Asher. ''Deep-Ultraviolet Resonance Raman Excitation Profiles of NH_4NO_3, PETN, TNT, HMX, and RDX''. Appl. Spectrosc. 2012. 66(9): 1013-1021.
12. A.W. Fountain III, S.D. Christesen, R.P. Moon, J.A. Guicheteau, E.D. Emmons. ''Recent Advances and Remaining Challenges for the Spectroscopic Detection of Explosive Threats''. Appl. Spectrosc. 2014. 68(8): 795-811.
13. E.D. Emmons, A. Tripathi, J.A. Guicheteau, A.W. Fountain III, S.D. Christesen. ''Ultraviolet Resonance Raman Spectroscopy of Explosives in Solution and the Solid State''. J. Phys. Chem. A. 2013. 117(20): 4158-4166.
14. S.D. Christesen, A.W. Fountain III, E.D. Emmons, J.A. Guicheteau. ''Raman Detection of Explosives''. In: P.M. Pellegrino, E.L. Holthoff, M.E. Farrell, editors. Laser-Based Optical Detection of Explosives. Boca Raton, FL: CRC Press, 2015. Pp. 99-122.
15. J.R. O'Connor. ''Unusual Crystal-Field Energy Levels and Efficient Laser Properties of YVO_4:Nd''. Appl. Phys. Lett. 1966. 9(11): 407-409.
16. L. DeShazer. ''Vanadate Crystals Exploit Diode-Pump Technology''. Laser Focus World. 1994. 30: 88-93.
17. S.V. Bykov, B. Sharma, S.A. Asher. ''High-Throughput, High-Resolution Echelle Deep-UV Raman Spectrometer''. Appl. Spectrosc. 2013. 67(8): 873-883.
18. S.A. Asher, C.R. Johnson, J. Murtaugh. ''Development of a New UV Resonance Raman Spectrometer for the 217-400 nm Spectral Region''. Rev. Sci. Instrum. 1983. 54: 1657-1662.
19. S. Bykov, I. Lednev, A. Ianoul, A. Mikhonin, C. Munro, S.A. Asher. ''Steady-State and Transient Ultraviolet Resonance Raman Spectrometer for the 193–270 nm Spectral Region''. Appl. Spectros. 2005. 59(12): 1541-1552.
20. S.A. Asher, D.D. Tuschel, T.A. Vargson, L. Wang, S.J. Geib. ''Solid State and Solution Nitrate Photochemistry: Photochemical Evolution of the Solid State Lattice''. J. Phys. Chem. A. 2011. 115(17): 4279-4287.
21. S. Chaturvedi, P.N. Dave. ''Review on Thermal Decomposition of Ammonium Nitrate''. J. Energ. Mater. 2013. 31(1): 1-26.
22. M. Lax. ''Temperature Rise Induced by a Laser Beam''. J. Appl. Phys. 1977. 48(9): 3919-3924.